

# Graphene-TMDC-Graphene Hybrid Plasmonic Metasurface for Enhanced Biosensing: A Theoretical Analysis

Li Jiang, Shuwen Zeng,\* Qingling Ouyang, Xuan-Quyen Dinh, Philippe Coquet, Junle Qu, Sailing He,\* and Ken-Tye Yong\*

In this work, a plasmonic metasurface for ultra-sensitive biosensing based on graphene-transition metal dichalcogenide (TMDC)-graphene hybrid nanostructures are designed. The coating of the two-dimensional nanosheets plays an important role for the sensitivity enhancement of the biosensors at the atomic scale. To achieve the maximum plasmon resonance energy transfer, different parameters of the hybrid nanostructures are systematically investigated including the material types and the number of TMDC layers. The important characteristics of plasmonic biosensors such as dark minimum reflectivity, sharp differential phase change, high sensitivity and narrow full width at half maximum (FWHM) are carefully studied in this work to demonstrate the improved surface plasmon resonance sensing performances of the TMDC-based metasurfaces. The graphene-TMDC-graphene configurations with four different types of materials including  $\text{MoS}_2/\text{WS}_2/\text{MoSe}_2/\text{WSe}_2$  are optimized respectively for potential sensing applications. Based on our theoretical analysis, the enhanced maximum sensitivity of graphene-TMDC-graphene hybrid nanostructure is three orders of magnitude higher than that of the conventional bare metallic substrate.

## 1. Introduction

For the last decade, surface plasmon resonance (SPR) sensor has been serving as a useful tool to monitor the interactions of biomolecules on the sensing surface in real-time.<sup>[1–3]</sup> The excited plasmon evanescent field is highly sensitive to even tiny refractive index changes ( $10^{-6}$  RIU) induced by the interactions between the molecules at the interface. Thus, the signal parameters of the reflected light from the sensing surface such as intensity and phase have sharp changes due to the mismatch of the resonance condition. These signal changes are usually proportional to the concentration of the biomolecules in the sample solutions. Such unique ability of SPR sensors allows one to quantitatively determine the dynamic kinetics and concentration of biomolecules in dilute samples. However, the conventional SPR sensors with bare metallic thin film currently face a great challenge in detecting the biomolecules with ultralow molar

concentration (typically less than 1 pM). Thus, the SPR sensing configurations with enhanced intensity and phase signal changes are needed to be explored and optimized to overcome this limitation. It is known that SPR effect shows typical physical properties as an abrupt phase jump, a prominent darkness of the reflected light, and a strongly enhanced plasmon electric field induced at the sensing interface.<sup>[2,4,5]</sup> Ideally, one needs to achieve a darker minimum reflectivity and a more enhanced electric field in order to improve the SPR excitation efficiency. In this case, most of the incident light energy up to 95% can be transferred into the plasmon resonance energy.<sup>[6]</sup>

Recent studies have employed two-dimensional (2D) nanomaterials<sup>[7–10]</sup> (i.e., transition metal dichalcogenides (TMDCs),<sup>[11–14]</sup> grapheme,<sup>[15–17]</sup> and graphene analogues<sup>[18,19]</sup>) to enhance the plasmonic sensing performances.<sup>[2,20]</sup> In general, TMDCs family show a chemical formula of  $\text{MX}_2$  and a sandwich structure of X-M-X, where M stands for transition element (i.e.,  $\text{M} = \text{Cr}, \text{Mo}, \text{W}$ ) and X stands for chalcogen element (i.e.,  $\text{X} = \text{S}, \text{Se}, \text{Te}$ ).<sup>[21]</sup> Graphene and TMDCs are 2D layered materials with atomic thickness, and can be stacked layer by layer due to van der Waals interactions. This feature gives the possibility that the plasmonic sensing performance can be tuned at the atomic scale. Moreover, strong light-matter interaction has been demonstrated as a generic


L. Jiang, Prof. S. He  
State Key Laboratory of Modern Optical Instrumentation  
Centre for Optical and Electromagnetics Research  
JORCEP (Sino-Swedish Joint Research Center of Photonics)  
Zhejiang University  
310058 Hangzhou, P. R. China  
E-mail: sailing@kth.se

L. Jiang, Dr. S. Zeng, Q. Ouyang, Prof. K.-T. Yong  
School of Electrical and Electronic Engineering  
Nanyang Technological University  
639798 Singapore, Singapore  
E-mail: swzeng@ntu.edu.sg; ktyong@ntu.edu.sg

L. Jiang, Dr. S. Zeng, Q. Ouyang, Dr. X.-Q. Dinh, Prof. P. Coquet  
CINTRA CNRS/NTU/THALES, UMI 3288  
Research Techno Plaza  
50 Nanyang Drive, Border X Block, 637553 Singapore, Singapore

Prof. P. Coquet  
Institut d'Electronique, de Microélectronique et de Nanotechnologie  
(IEMN) CNRS UMR 8520–Université de Lille 1  
59650 Villeneuve d'Ascq, France

Prof. J. Qu  
College of Optoelectronic Engineering  
Shenzhen University  
Key Laboratory of Optoelectronic Devices and Systems of Ministry of Education and Guangdong Province  
Shenzhen, 518060 Guangdong, P. R. China

 The ORCID identification number(s) for the author(s) of this article can be found under <https://doi.org/10.1002/pssa.201700563>.

DOI: 10.1002/pssa.201700563

feature for monolayer TMDCs due to Van Hove singularities observed in their density of states peaks.<sup>[22–24]</sup> The light absorption rates of the TMDC monolayers are found to be around 5% to 10%, and the one of graphene is 2.3%,<sup>[25,26]</sup> which can transfer more energy to afford the electronic resonant.

In this work, we have engineered hybrid G-TMDC-G (G stands for monolayer graphene) nanostructure onto a metal thin film as an enhanced plasmonic biosensing platform. Here, the metal thin film provides abundant free electrons to generate surface plasmon polaritons. The effects of hybrid nanostructure can be well demonstrated from three aspects: (i) the top layer graphene is acting as capture units to adsorb biomolecules with aromatic ring structure that is originated from pi-stacking interaction process<sup>[2]</sup>; (ii) it has a high surface-to-volume ratio that allows sufficient adsorption of target biomolecules<sup>[27–31]</sup>; (iii) the coating of hybrid nanostructure on the sensing surface can effectively prevent the lower metal thin film (especially for silver) from oxidation and corrosion.<sup>[17]</sup> In this work, our analysis reveals that the real part and imaginary part of the refractive index as well as the thickness of the coating materials play important roles in affecting the dispersion relation of surface plasmon oscillations, which determines the minimum reflectivity.<sup>[32]</sup> Four types of TMDC materials<sup>[33–38]</sup> have been investigated systematically in this study including molybdenum disulfide (MoS<sub>2</sub>), Tungsten disulfide (WS<sub>2</sub>), Molybdenum diselenide (MoSe<sub>2</sub>) and tungsten diselenide (WSe<sub>2</sub>) with different numbers of layers. Based on our results, G-WS<sub>2</sub>-G hybrid nanostructure coated on the 42 nm Ag thin film coupled by a ZnSe prism shows the darkest minimum reflectivity and highest phase sensitivity at the 632.8 nm excitation wavelength. The enhancement factor of the hybrid plasmonic metasurface is at least three orders magnitude higher than that of the one with the bare Ag thin film and Ag thin film coated with monolayer graphene.

## 2. Theoretical Methods

Our theoretical analysis is based on a N-layer model consisted of prism, metal, monolayer graphene, TMDCs, monolayer graphene and biomolecules, as shown in **Figure 1**. The number of N-layer model is 6 ( $N=6$ ), and all materials are stacked layer by layer and assumed to be optically isotropic and non-magnetic. Titanium serves as an adhesion layer with a thickness of 2.5 nm

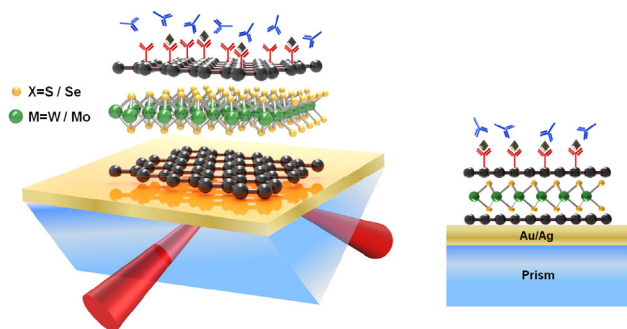


**Figure 1.** Schematic diagram of SPR biosensor based on G-TMDC-G/metal hybrid multilayer sensing substrate.

at the bottom of metal thin film. Here, the nomenclature for the hybrid multilayer sensing substrate is defined as “G-TMDC-G/metal” for better descriptions.

To optimize G-TMDC-G hybrid nanostructure with the best sensing performance, TMDC materials of MoS<sub>2</sub>, WS<sub>2</sub>, MoSe<sub>2</sub>, and WSe<sub>2</sub> from monolayer to 5-layer have been investigated systematically. The wavelengths of SPR excitation light vary from visible to near infrared (NIR) range including 632.8, 785, 980, and 1550 nm. These wavelengths have been widely used in the conventional SPR configuration due to the low cost for the laser source.<sup>[39–44]</sup> Au and Ag thin film, as the plasmonic metals, provide a negative real permittivity at the dielectric/metal interface with the abundance of free electrons. The wave vector of the excitation light is determined by the coupling prism with different materials including BK7, SF11, 2S2G, ZnSe, and silicon (only for 1550 nm). Silica based prisms (BK7 and SF11) are mostly common applied in the conventional SPR sensing configurations. ZnSe prism with higher refractive index than silica prisms, has a large potential tuning range to realize wide dynamic range of SPR measurement and retains adequate transmission rate for the wavelength from visible to infrared range.<sup>[45,46]</sup> Chalcogenide glass (2S2G) offers a large operating window due to the good transparent behavior in the near-to mid-infrared region.<sup>[47,48]</sup> In the NIR range, the standard doped silicon is transparent enough for the SPR coupling while the transmission rate is zero in the visible range.<sup>[49]</sup>

Transfer matrix method (TMM) and Fresnel equations are employed to calculate the SPR sensing characteristics of the hybrid multilayer sensing substrate, including minimum reflectivity ( $R_{\min}$ ), resonance angle ( $\theta_{\text{SPR}}$ ), differential phase change ( $\Delta\theta_d$ ), phase sensitivity ( $S_p$ ) and the full width at half of maximum (FWHM). The simulation parameters of each layer are defined by thickness  $d_m$ , refractive index  $n_m$  and dielectric function  $\epsilon_m$ . The refractive index and dielectric function of all the materials at different wavelengths are shown in Tables S1 and S2 (Supporting Information). The thickness of monolayer graphene and monolayer TMDCs (MoS<sub>2</sub>, WS<sub>2</sub>, MoSe<sub>2</sub>, WSe<sub>2</sub>) are listed in Table S3 (Supporting Information). The tangential component of the electromagnetic field at the interface of the first layer ( $z=0$ ) and the last layer ( $z=N-1$ ) boundary relate with the following equation,

$$\begin{bmatrix} E_1^T \\ H_1^T \end{bmatrix} = M \cdot \begin{bmatrix} E_{N-1}^T \\ H_{N-1}^T \end{bmatrix} \quad (1)$$

$M$  in Eq. (1) is the Transfer Matrix (TM) of the combined N-layer which is given by Eq. (2),

$$M = \begin{bmatrix} M_{11} & M_{12} \\ M_{21} & M_{22} \end{bmatrix} = \prod_{m=2}^{N-1} \begin{bmatrix} \cos\beta_m & -\frac{i(\sin\beta_m)}{q_m} \\ -i(\sin\beta_m) \cdot q_m & \cos\beta_m \end{bmatrix} \quad (2)$$

with

$$q_m = \frac{\sqrt{\epsilon_m - n_1^2 \sin^2 \theta}}{\epsilon_m} \quad (3)$$

$$\beta_m = \frac{2\pi d_m}{\lambda_0} \sqrt{\epsilon_m - n_1^2 \sin^2 \theta} \quad (4)$$

$\theta$  in Eqs. (3) and (4) represents the incident angle at the base of coupling prism with the refractive index of  $n_1$ .

The Fresnel reflection coefficient for TM-polarized light is given by Eq. (5),

$$\phi_p = \arg(r_p) \quad (5)$$

and

$$q_m = \sqrt{\epsilon_m - n_1^2 \sin^2 \theta} \quad (6)$$

The differential phase change between TM-polarized and TE-polarized light is obtained by Eq. (7),

$$\phi_d = |\phi_p - \phi_s| \quad (7)$$

Reflectivity ( $R_p$ ) is plotted as a function of incident angle ( $\theta_{inc}$ ) where the minimum reflectivity ( $R_{min}$ ) corresponds to the resonance angle ( $\theta_{SPR}$ ). The intensity of the reflected light at this resonance angle is normally near to zero, called a point of darkness. Also, an abrupt phase change occurs at the resonance angle. It is known that the phase change becomes sharper when the minimum reflectivity is darker. Therefore, a sharp differential phase change ( $\Delta\phi_d$ ) can be detected at the resonance condition due to even a tiny refractive index change of biomolecule sample solutions injected into the sensing chamber when  $\theta_{SPR}$  is fixed. With the change of differential phase  $\Delta\phi_d$  corresponding to the refractive index change  $\Delta n$ , the phase sensitivity is defined as Eq. (8),

$$S_p = \frac{\Delta\phi_d}{\Delta n} \quad (8)$$

In this work, the phase sensitivity is only analyzed for the linear relationship between differential phase change and refractive index change.

The full width at half maximum (FWHM) can be used to evaluate the SPR sensing accuracy, which can be defined as the width of the curve at the half of maximum reflectivity  $R_{FWHM}$  as given in Eq. (9),

$$R_{FWHM} = \frac{1}{2}(R_{min} + R_{max}) \quad (9)$$

here,  $R_{min}$  and  $R_{max}$  represent the minimum and maximum reflectivity, respectively.

### 3. Results and Discussion

All the SPR sensing characteristics (i.e., minimum reflectivity, differential phase change, phase sensitivity, and FWHM) are calculated and considered in the optimization of G-TMDC-G hybrid nanostructures for the bio- and chemical application. In our theoretical analysis, optimized structures for various TMDC materials with various layers coated on Au or Ag thin film with different thicknesses coupled by various prisms at different excitation wavelengths have been studied. Among these combinations, optimized groups for MoS<sub>2</sub>, WS<sub>2</sub>, MoSe<sub>2</sub>, and WSe<sub>2</sub> are specifically selected and listed in Tables 1–4. All the other detailed results are shown in Tables S4 to S11 (Supporting Information). In the tables,  $\theta_{SPR}$  represents resonance angle for pure water.  $\Delta\theta_{SPR}$  is the change in resonance angle caused by 0.12 RIU refractive index change due to biomolecules absorption.  $\Delta\phi_d$  gives the differential phase change between TM-polarized and TE-polarized light for refractive index change of 10<sup>-6</sup> RIU and 0.0012 RIU, respectively. In each optimized group, resonance angle decreases as the coupling prism with the higher refractive index due to the wavevector matching condition for SPR excitation. However, resonance angle shows only slight changes with various excitation wavelengths. Also, infrared excitation wavelength coupled with the Ag thin film shows narrower FWHM, which is attributed by the larger real part of the permittivity of Ag thin film. This narrower FWHM represents higher SPR sensing accuracy. The change in differential phase shows a linear relationship with tiny refractive index change (from 10<sup>-7</sup>U to 10<sup>-6</sup> RIU) caused by the capture biomolecules, and becomes saturated as the refractive index change increases to 0.0012 RIU. In general, the refractive index

**Table 1.** Optimized groups for MoS<sub>2</sub> at various excitation wavelengths show various SPR characteristics based on G-MoS<sub>2</sub>-G/metal hybrid sensing substrate.

$\lambda$ (nm)	Metal	Prism	$d_{metal}$ (nm)	MoS <sub>2</sub> layers	$\theta_{SPR}$ (°) w/o molecule	$\Delta\theta_{SPR}$ (°) ( $\Delta n_{bio} = 0.12$ )	$\Delta\phi_d$ (°) ( $\Delta n_{bio} = 10^{-6}$ )	$\Delta\phi_d$ (°) ( $\Delta n_{bio} = 0.0012$ )	$S_p$ (°/RIU)	FWHM (°)	$R_{min}$
1550	Au	SF11	27	5	49.91	0.21	0.06	54.14	$6.55 \times 10^4$	0.1754	$2.76 \times 10^{-5}$
980	Au	BK7	40	5	65.89	1.06	0.40	83.53	$4.04 \times 10^5$	0.7224	$1.29 \times 10^{-6}$
785	Au	2S2G	41	4	38.03	0.65	0.17	75.06	$1.73 \times 10^5$	0.5024	$5.26 \times 10^{-6}$
632.8	Au	SF11	30	4	61.38	2.76	0.06	54.75	$6.74 \times 10^4$	7.5415	$2.33 \times 10^{-6}$
1550	Ag	SF11	38	1	49.51	0.16	14.80	119.78	$1.48 \times 10^7$	0.0371	$9.21 \times 10^{-9}$
980	Ag	SF11	45	2	50.63	0.46	1.28	88.74	$1.28 \times 10^6$	0.0931	$1.50 \times 10^{-6}$
785	Ag	SF11	44	4	52.22	0.90	5.65	89.84	$5.65 \times 10^6$	0.2690	$3.27 \times 10^{-8}$
632.8	Ag	SF11	44	0	52.45	1.25	2.34	90.40	$2.34 \times 10^6$	0.3595	$1.85 \times 10^{-7}$

**Table 2.** Optimized groups for WS<sub>2</sub> under various excitation wavelengths show various SPR characteristics based on G-WS<sub>2</sub>-G/metal hybrid sensing substrate.

$\lambda$ (nm)	Metal	Prism	$d_{\text{metal}}$ (nm)	WS <sub>2</sub> layers	$\theta_{\text{SPR}}(^{\circ})$ w/o molecule	$\Delta\theta_{\text{SPR}}(^{\circ})$ ( $\Delta n_{\text{bio}} = 0.12$ )	$\Delta\theta_{\text{d}}(^{\circ})$ ( $\Delta n_{\text{bio}} = 10^{-6}$ )	$\Delta\theta_{\text{d}}(^{\circ})$ ( $\Delta n_{\text{bio}} = 0.0012$ )	$S_{\text{p}}$ ( $^{\circ}/\text{RIU}$ )	FWHM ( $^{\circ}$ )	$R_{\text{min}}$
1550	Au	SF11	27	2	49.80	0.20	2.10	86.34	$2.10 \times 10^6$	0.1946	$2.75 \times 10^{-8}$
980	Au	SF11	36	4	51.81	0.64	0.32	81.61	$3.21 \times 10^5$	0.5646	$1.27 \times 10^{-6}$
785	Au	SF11	42	4	53.57	1.14	0.36	82.68	$3.63 \times 10^5$	0.7862	$1.44 \times 10^{-6}$
632.8	Au	2S2G	40	1	39.04	1.16	0.86	86.52	$8.63 \times 10^5$	1.2560	$9.08 \times 10^{-8}$
1550	Ag	Si	42	0	22.42	0.05	0.89	90.91	$8.96 \times 10^5$	0.0110	$3.21 \times 10^{-6}$
980	Ag	SF11	40	5	51.37	0.57	0.84	88.25	$8.45 \times 10^5$	0.2158	$1.01 \times 10^{-6}$
785	Ag	ZnSe	47	1	33.07	0.39	1.41	86.85	$1.41 \times 10^6$	0.0802	$1.10 \times 10^{-6}$
632.8	Ag	ZnSe	42	1	33.28	0.68	21.12	86.85	$2.11 \times 10^7$	0.2576	$1.14 \times 10^{-9}$

change is determined by the molecular weight and molar concentration of the capture biomolecules. More importantly, the theoretical results demonstrate that the higher phase sensitivity corresponds to the darker minimum reflectivity. This is because that the phase accumulates more sharply at the darker point of the reflected intensity.

In our models, the optimized hybrid nanostructures for SPR sensing configuration need to provide dark minimum reflectivity, high sensitivity, and sharp differential phase change together with narrow FWHM. Among all the optimized groups, G-WS<sub>2</sub>-G/Ag hybrid sensing substrate coupled by ZnSe prism, with monolayer WS<sub>2</sub> and 42 nm Ag thin film, shows the best SPR performance with the excitation wavelength of 632.8 nm.

**Figure 2** gives SPR reflectivity and phase curves of TM-polarized light based on G-WS<sub>2</sub>-G/Ag hybrid sensing substrates, which shows five main features: (i) the minimum reflectivity of TM-polarized light under SPR condition corresponds to an abrupt phase change; (ii) the sharpest phase change of TM-polarized light takes place when the minimum reflectivity is close to zero.

**Figure 3** exhibits that the sharpest phase change is related to a lowest minimum reflectivity of  $1.14 \times 10^{-9}$ ; (iii) the darkness of the minimum reflectivity strongly depends on the number of WS<sub>2</sub> layer in the G-WS<sub>2</sub>-G/Ag hybrid sensing substrate. The

absorption of the incident light and the energy loss of the damping should be taken into consideration when increasing number of WS<sub>2</sub> layer. More absorption of the incident light while less energy loss of the damping is required for a SPR excitation with high efficiency. Thus, there is a trade-off balance to choose the number of WS<sub>2</sub> layer; (iv) The SPR resonance angle ( $\theta_{\text{SPR}}$ ) has a relatively large red shift with increasing number of WS<sub>2</sub> layers at fixed sensing substrate parameters, since the real part of the dielectric constant of the hybrid nanostructure increases as the number of WS<sub>2</sub> layer increases, which results in the increased SP wave vector; (v) The increase number of WS<sub>2</sub> layer widen FWHM, which is attributed to the energy loss of electrons due to the large imaginary part of WS<sub>2</sub> dielectric function.

In order to compare the SPR sensing performance based on phase-interrogation and angular-interrogation, differential phase change ( $\Delta\theta_{\text{d}}$ ) and resonance angle change ( $\Delta\theta_{\text{SPR}}$ ) corresponding to a refractive index change ( $\Delta n_{\text{bio}} = 0.0012$  RIU or  $\Delta n_{\text{bio}} = 0.12$  RIU) due to the absorption of biomolecules are plotted with respect to silver thickness from 30 to 50 nm, as shown in **Figure 4a** and **b**. The obvious change in differential phase is more than 10 degree and less than 90 degree for the refractive index change of 0.0012 RIU, with the phase sensitivity from 8333 deg/RIU to 75 000 deg/RIU. The change in resonance

**Table 3.** Optimized groups for MoSe<sub>2</sub> under various excitation wavelengths show various SPR characteristics based on G-MoSe<sub>2</sub>-G/metal hybrid sensing substrate.

$\lambda$ (nm)	Metal	Prism	$d_{\text{metal}}$ (nm)	MoSe <sub>2</sub> layers	$\theta_{\text{SPR}}(^{\circ})$ w/o molecule	$\Delta\theta_{\text{SPR}}(^{\circ})$ ( $\Delta n_{\text{bio}} = 0.12$ )	$\Delta\theta_{\text{d}}(^{\circ})$ ( $\Delta n_{\text{bio}} = 10^{-6}$ )	$\Delta\theta_{\text{d}}(^{\circ})$ ( $\Delta n_{\text{bio}} = 0.0012$ )	$S_{\text{p}}$ ( $^{\circ}/\text{RIU}$ )	FWHM ( $^{\circ}$ )	$R_{\text{min}}$
1550	Au	2S2G	27	4	36.29	0.13	0.99	89.06	$9.93 \times 10^5$	0.1286	$1.16 \times 10^{-7}$
980	Au	2S2G	35	5	37.24	0.37	0.23	78.91	$2.36 \times 10^5$	0.3378	$2.23 \times 10^{-6}$
785	Au	2S2G	38	2	37.59	0.58	0.16	73.94	$1.60 \times 10^5$	0.5243	$4.59 \times 10^{-6}$
632.8	Au	2S2G	38	1	38.91	1.14	0.54	85.92	$5.39 \times 10^5$	1.3992	$1.81 \times 10^{-7}$
1550	Ag	BK7	38	4	62.31	0.28	16.41	98.99	$1.64 \times 10^7$	0.0772	$5.59 \times 10^{-9}$
980	Ag	BK7	45	2	64.22	0.78	1.47	85.62	$1.47 \times 10^6$	0.1762	$8.83 \times 10^{-7}$
785	Ag	2S2G	47	0	36.61	0.42	1.01	84.27	$1.01 \times 10^6$	0.0826	$2.39 \times 10^{-6}$
632.8	Ag	SF11	44	0	52.46	1.25	2.34	90.40	$2.34 \times 10^6$	0.3595	$1.86 \times 10^{-7}$

**Table 4.** Optimized groups for WSe<sub>2</sub> under various excitation wavelengths show various SPR characteristics based on G-WSe<sub>2</sub>-G/metal hybrid sensing substrate.

$\lambda$ (nm)	Metal	Prism	$d_{\text{metal}}$ (nm)	WSe <sub>2</sub> layers	$\theta_{\text{SPR}}(^{\circ})$ w/o molecule	$\Delta\theta_{\text{SPR}}(^{\circ})$ ( $\Delta n_{\text{bio}}=0.12$ )	$\Delta\theta_d(^{\circ})$ ( $\Delta n_{\text{bio}}=10^{-6}$ )	$\Delta\theta_d(^{\circ})$ ( $\Delta n_{\text{bio}}=0.0012$ )	$S_p$ ( $^{\circ}$ /RIU)	FWHM ( $^{\circ}$ )	$R_{\text{min}}$
1550	Au	SF11	27	2	49.79	0.19	0.52	84.64	$5.22 \times 10^5$	0.1918	$4.51 \times 10^{-7}$
980	Au	2S2G	36	5	37.35	0.38	2.38	91.62	$2.38 \times 10^6$	0.3424	$2.32 \times 10^{-8}$
785	Au	2S2G	42	4	38.01	0.65	1.56	89.37	$1.56 \times 10^6$	0.4559	$7.81 \times 10^{-8}$
632.8	Au	SF11	35	5	62.63	3.25	0.17	73.26	$1.70 \times 10^5$	6.0145	$7.41 \times 10^{-7}$
1550	Ag	Si	41	2	22.45	0.06	2.69	98.77	$2.69 \times 10^6$	0.0132	$2.82 \times 10^{-7}$
980	Ag	SF11	45	1	50.53	0.44	5.42	85.25	$5.42 \times 10^6$	0.0878	$8.48 \times 10^{-8}$
785	Ag	2S2G	46	3	37.06	0.50	2.65	88.64	$2.65 \times 10^6$	0.1188	$2.36 \times 10^{-7}$
632.8	Ag	SF11	44	0	52.45	1.25	2.34	90.40	$2.34 \times 10^6$	0.3595	$1.86 \times 10^{-7}$

angle is about one degree for the refractive index change of 0.12 RIU, with the angular sensitivity near 8.333 deg/RIU. Therefore, phase-interrogation shows 3–4 orders higher sensitivity than angular-interrogation due to an abrupt phase change at a fixed resonance angle. Curves of FWHM and minimum reflectivity under the SPR effect of pure water at the 632.8 nm wavelength are plotted with respect to the thickness of Ag thin film as well, as shown in Figure 4c and d. The resonance angle and FWHM change with the number of WS<sub>2</sub> layer, since the real part of effective dielectric function of G-WS<sub>2</sub>-G/Ag hybrid sensing substrate is determined by the number of WS<sub>2</sub> layer. Change in differential phase and minimum reflectivity for various numbers of WS<sub>2</sub> layer further demonstrate that minimum reflectivity is related to a sharp phase change. The hybrid sensing substrates, 42 nm Ag thin film with monolayer WS<sub>2</sub>, 35 nm Ag thin film with 5-layer WS<sub>2</sub>, 40 nm Ag thin film with bilayer WS<sub>2</sub>, exhibit significant differential phase changes. WS<sub>2</sub> mentioned here is sandwiched by monolayer graphene as described above. Among all the optimized sensing schemes, 42 nm Ag thin film with monolayer WS<sub>2</sub> is the best sensing configuration with a significant differential phase change of 86.85°, a narrow FWHM of 0.2576° and a dark minimum reflectivity of  $1.14 \times 10^{-9}$ .

To investigate the effect of WS<sub>2</sub> layers in the G-WS<sub>2</sub>-G hybrid nanostructure, the thickness of Ag thin film is fixed at 42 nm, and the number of WS<sub>2</sub> is tuned from monolayer to 5

layers. As shown in Figure 5a, monolayer WS<sub>2</sub> in the G-WS<sub>2</sub>-G hybrid nanostructure exhibits the most significant differential phase change that has 10 times higher than the one based on bilayer WS<sub>2</sub>.

This abrupt phase change is caused by the ultrahigh sensitivity of G-WS<sub>2</sub>(1)-G/Ag(42 nm) hybrid sensing substrate. Moreover, change in differential phase of monolayer WS<sub>2</sub> based nanostructure starts to saturate at the refractive index of 1.3327, while the one of bilayer WS<sub>2</sub> based nanostructure maintains good linear relationship with the refractive index of 1.3338. This is because monolayer WS<sub>2</sub> based nanostructure shows superior sensitivity to the slight refractive index change of biomolecules over bilayer WS<sub>2</sub> based nanostructure. Obviously, monolayer WS<sub>2</sub> based nanostructure possesses high sensitivity in differential phase change with the expense of detection dynamic range. It is worth noting that the phase sensitivity is defined within the linear range that the differential phase change is linearly related with the refractive index. Thus, a tiny refractive index change induced by absorption of biomolecules on the sensing surface as low as  $10^{-7}$  RIU is used in our model to ensure the linear change of differential phase in Figure 5b. G-WS<sub>2</sub>-G hybrid nanostructure shows the most sensitive performance compared with structure based on bare Ag thin film or monolayer graphene. All the structures for comparison are coated on the Ag thin film with a fixed thickness of 42 nm.

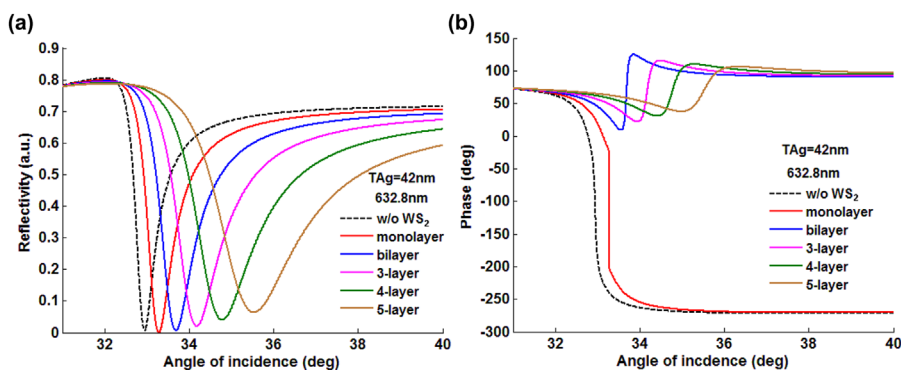


**Figure 2.** Curves of reflectivity (a) and phase (b) with respect to various incident angles based on G-WS<sub>2</sub>-G/Ag hybrid sensing substrates. The thickness of Ag thin film is 42 nm. DI water is attached on the sensing surface with a refractive index of 1.3326 at the excitation wavelength of 632.8 nm.

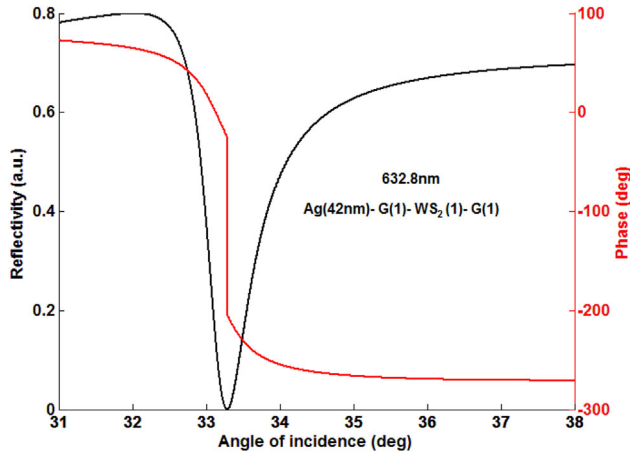


**Figure 3.** SPR sensing curves of reflectivity (black) and phase (red) related to different incident angles for DI water attached on the sensing surface with a refractive index of 1.3326 at the excitation wavelength of 632.8 nm. Ag thin film with the thickness of 42 nm is coated with the G-WS<sub>2</sub>(1)-G hybrid nanostructure (WS<sub>2</sub>(1) stands for monolayer WS<sub>2</sub>).

**Figure 6** shows the enhancement of SPR sensing performance based on various numbers of WS<sub>2</sub> layers and Ag thin film with different thicknesses. The plot of the ratio between differential phase change and refractive index change of

biomolecules ( $(\Delta\theta_{SPR})/(\Delta n_{bio})$ ) further demonstrates that the most optimal hybrid nanostructure is G-WS<sub>2</sub>(1)-G/Ag(42 nm) at the excitation wavelength of 632.8 nm as shown in Figure 6a. The thickness of Ag thin film is 42 nm and the number of WS<sub>2</sub> layer is monolayer. The plot of the ratio between SPR resonance angle change and refractive index change of biomolecules ( $(\Delta\theta_{SPR})/(\Delta n_{bio})$ ) in Figure 6b further demonstrates that the number of WS<sub>2</sub> layer directly influences the resonance angle due to the real part of effective dielectric function of the G-WS<sub>2</sub>-G/Ag hybrid sensing substrate. We also find that the sensing substrate exhibiting the most significant differential phase change is not corresponding to the largest SPR resonance angle change. This is because the differential phase is only determined by the darkness of the minimum reflectivity, but has no inherent relation with the position of the resonance angle.<sup>[4]</sup> Here, the absorption and real part of the effective dielectric function of the G-TMDC-G/Ag hybrid sensing substrate respectively determine the minimum reflectivity and resonance angle. The phase sensitivity within the refractive index change of 10<sup>-6</sup> RIU is depicted in Figure 6c. The maximum phase sensitivity for G-WS<sub>2</sub>(1)-G/Ag(42 nm) hybrid sensing substrate is up to  $2.11 \times 10^7$  °/RIU.

To further study the SPR performance of the designed G-WS<sub>2</sub>-G/Ag hybrid sensing substrate, we also have employed finite element analysis (FEA) method (COMSOL Multiphysics 5.0) to simulate the electric field distribution along the sensing surface at the resonance angle. The incident light (wavelength

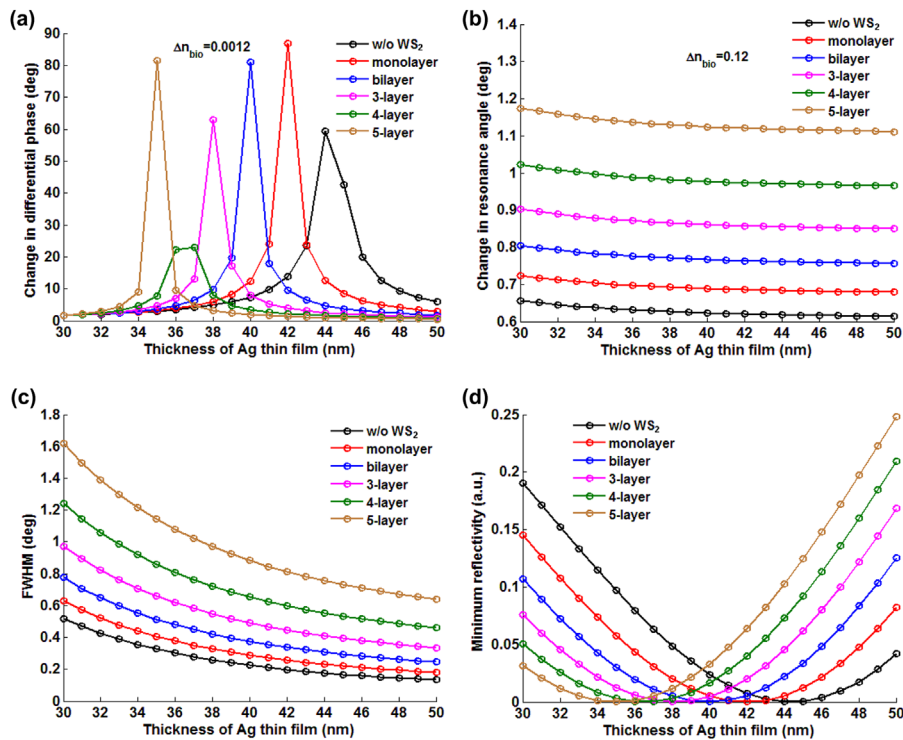


**Figure 4.** a) Differential phase change due to the refractive index change of 0.0012 RIU by absorption of biomolecules; b) change in SPR resonance angle with pure water on the sensing surface and a refractive index change of 0.12 RIU by absorption of biomolecules; c) FWHM; and d) Minimum reflectivity in SPR curve with pure water on the sensing surface. The curves are plotted with respect to Ag thickness from 30 to 50 nm at the wavelength of 632.8 nm. The circle symbols stand for the simulation results and the continuous lines are the fit curves through the circles symbols.

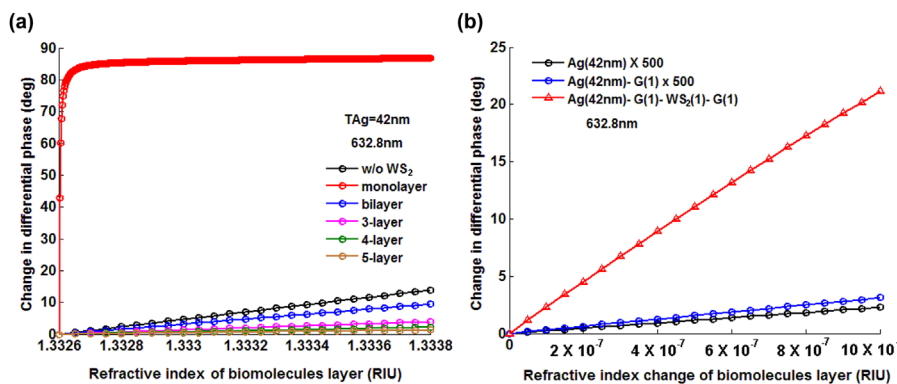


**Figure 5.** a) Variation of differential phase change with respect to refractive index of sample for different  $WS_2$  layers based on the G- $WS_2$ -G nanostructure. The thickness of Ag thin film is fixed at 42 nm and the excitation wavelength is 632.8 nm. (b) Comparison of change in differential phase for a trace of refractive index change of biomolecules layer as low as  $10^{-7}$  RIU based on G(1)- $WS_2$ (1)-G(1) (red), monolayer graphene (blue) coated on 42 nm Ag thin film, and bare 42 nm Ag thin film (black). The changes in differential change for bare Ag thin film (black) and Ag thin film with monolayer graphene (blue) are magnified 500 times for clear comparison.

of 632.8 nm) is coupled by ZnSe prism (refractive index of 2.593) to G- $WS_2$ (1)-G/Ag(42 nm) hybrid substrate to excite the SPR effect (Figure 7a). The 3D electric field distribution of the model is shown in Figure 7. The simulation results confirm that the electric field is strongly enhanced at the sensing surface of the hybrid substrate, which contributes to a high sensitivity to even tiny refractive index change of sample solutions. In addition, the intensity of the electric field

exponentially decays with the distance away from the sensing surface of the hybrid substrate. Numerical electric field distribution curve clearly indicates that the evanescent wave exponentially decays along the propagation direction of surface plasmon wave (Figure 7d).

In addition to the above results for the optimized sensing substrate based on G- $WS_2$ -G hybrid nanostructure, Figure 8 shows the change in differential phase and sensitivity based

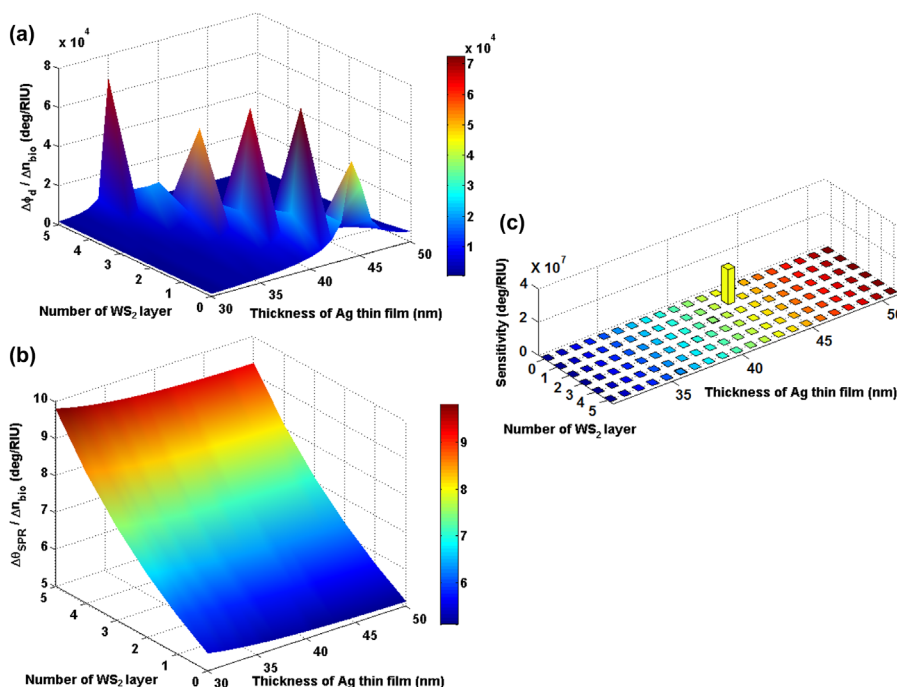


**Figure 6.** a) The ratio between differential phase change and refractive index change of biomolecules ( $\Delta n_{bio} = 0.0012$  RIU) absorbed on the sensing surface that as a function of number of  $WS_2$  layer and thickness of Ag thin film. (b) The ratio between change in SPR resonance angle and refractive index change of biomolecules ( $\Delta n_{bio} = 0.12$  RIU) for SPR excitation that as a function of number of  $WS_2$  layer and thickness of Ag thin film. (c) The phase sensitivity within the refractive index change of  $10^{-6}$  RIU that as a function of number of  $WS_2$  layer and thickness of Ag thin film. The excitation wavelength is 632.8 nm.

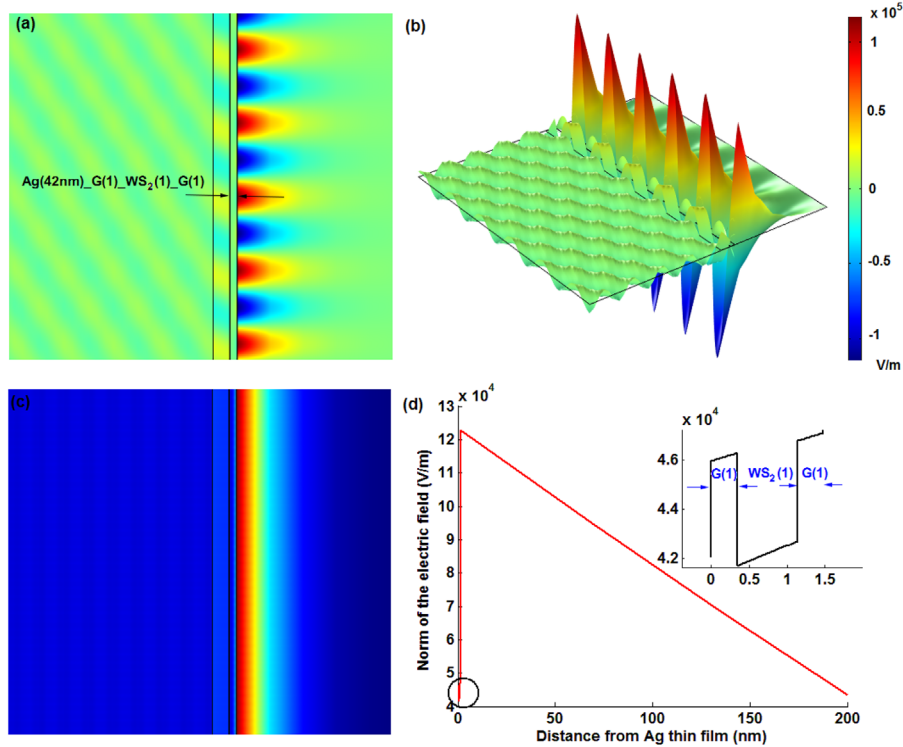


**Figure 7.** The FEA simulations of the electric field based on G-WS<sub>2</sub>-G hybrid nanostructure. a) 2D and (b) 3D electric field distribution at the resonance angle. c) The total electric field distributions showing enhanced filed on the G-WS<sub>2</sub>-G/Ag sensing surface. d) Numerical analysis of electric field across the structure from the Ag thin film. The value marked by the black circle is shown in the upper-right corner. The number of WS<sub>2</sub> is monolayer, and the thickness of Ag thin film is 42 nm. The coupling prism is ZnSe with the refractive index of 2.5930 under 632.8 nm excitation wavelength.

on the optimized G-MoS<sub>2</sub>-G, G-MoSe<sub>2</sub>-G, G-WSe<sub>2</sub>-G hybrid nanostructures, respectively. Figure 8a compares the change in differential phase between G-MoS<sub>2</sub>(1)-G/Ag(38 nm) hybrid sensing substrate (red curve), monolayer graphene coated on 38 nm Ag thin film (blue curve) and 38 nm bare Ag thin film (black curve). The sensitivity for the G-MoS<sub>2</sub>-G hybrid nanostructure is given in Figure 8b. In our case, the highest sensitivity is achieved as  $1.48 \times 10^7$ /RIU based on the G-MoS<sub>2</sub>(1)-G/Ag(38 nm) hybrid sensing substrate with 1550 nm excitation wavelength and SF11 coupling prism (Figure S1–S5 (Supporting Information)). Similarly, Figure 8c–e compare the differential phase change results for the G-MoSe<sub>2</sub>(4)-G/Ag(38 nm) and G-WSe<sub>2</sub>(5)-G/Au(36 nm) hybrid sensing substrates respectively. The corresponding sensitivity is respectively determined to be  $1.64 \times 10^7$  and  $2.38 \times 10^6$ /RIU (Figure 8d and f). The excitation wavelength

for G-MoSe<sub>2</sub>(4)-G/Ag(38 nm) hybrid sensing substrate is 1550 nm and the coupling prism is BK7. The excitation wavelength for G-WSe<sub>2</sub>(5)-G/Au(36 nm) hybrid sensing substrate is 980 nm and the coupling prism is 2S2G. Figure S6–S15 (Supporting Information) show the SPR sensing performances for both G-MoSe<sub>2</sub>(4)-G/Ag(38 nm) and G-WSe<sub>2</sub>(5)-G/Au(36 nm) hybrid sensing substrates, respectively. The enhancement factor of differential phase signal change compared with monolayer graphene coated on the metal thin film and the phase sensitivity for the hybrid substrates based on four types of TMDC materials are listed in Table 5. The changes in differential phase based on the G-TMDC-G hybrid nanostructures show 500–3000 times higher than the ones based on monolayer graphene. The comparison results demonstrate that G-TMDC-G hybrid metasurfaces can significantly enhance the SPR sensing

**Table 5.** The comparison of optimized results for four types of hybrid structures based on TMDC material of WS<sub>2</sub>, MoS<sub>2</sub>, MoSe<sub>2</sub> and WSe<sub>2</sub>.

$\lambda$ (nm)	Prism	Hybrid structure	$\Delta\theta_d(^{\circ})$ (G-TMDC-G)	$\Delta\theta_d(^{\circ})$ (G)	Enhancement factor	Sensitivity ( $^{\circ}$ /RIU)
632.8	ZnSe	Ag(42 nm)-G-WS <sub>2</sub> (1)-G	21.1233	0.0062	$3.4 \times 10^3$	$2.1123 \times 10^7$
1550	SF11	Ag(42 nm)-G-WS <sub>2</sub> (1)-G	14.8071	0.0208	$7.1 \times 10^2$	$1.4807 \times 10^7$
1550	BK7	Ag(42 nm)-G-WS <sub>2</sub> (1)-G	16.4098	0.0208	$1.5 \times 10^3$	$1.6410 \times 10^7$
980	2S2G	Ag(42 nm)-G-WS <sub>2</sub> (1)-G	2.3793	0.0208	$5.5 \times 10^2$	$2.3793 \times 10^6$



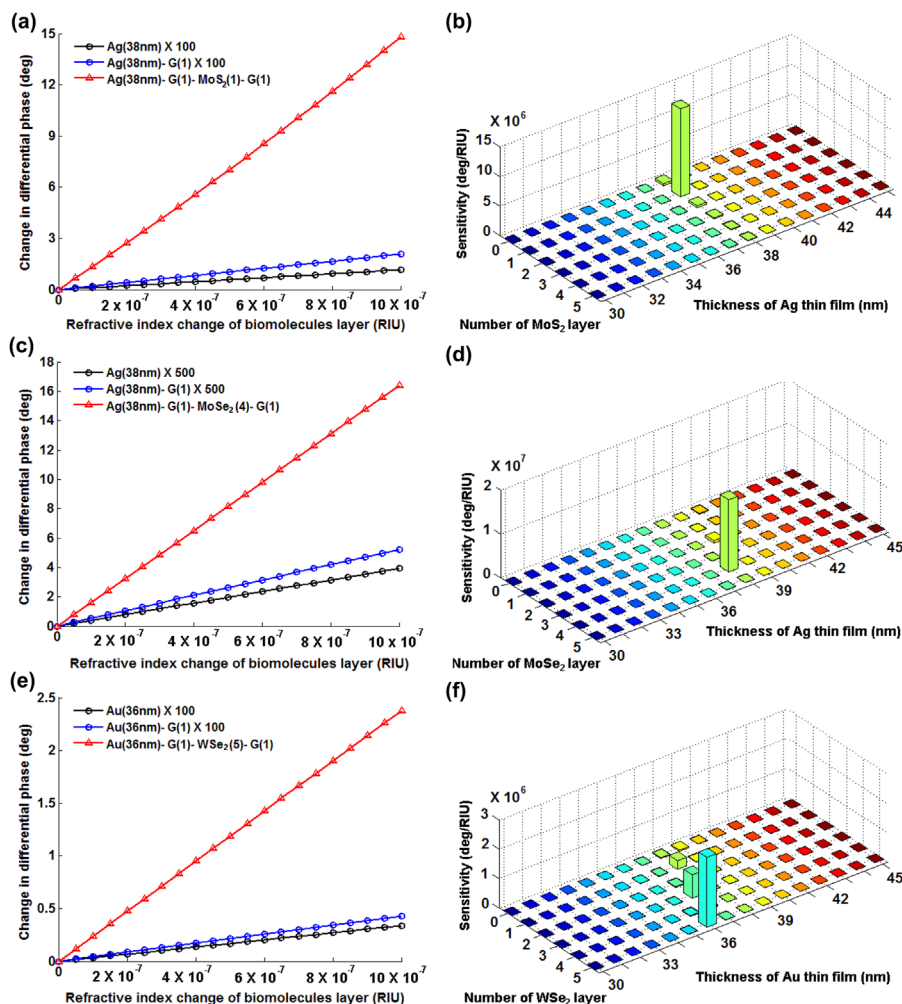


**Figure 8.** Comparison of change in differential phase for a trace of refractive index change of biomolecules layer as low as  $10^{-7}$  RIU based on (a) G-MoS<sub>2</sub>(1)-G/Ag(38 nm), (c) G-MoSe<sub>2</sub>(4)-G/Ag(38 nm), and (e) G-WSe<sub>2</sub>(5)-G/Au(36 nm) hybrid sensing substrates. The blue curves represent the one based on monolayer graphene coated Ag (Au) thin film and the black curves show the one based on bare Au (Ag) thin film. The two curves are magnified of 100 or 500 times for clear comparison. The phase sensitivity within the refractive index change of  $10^{-6}$  RIU that as a function of the number of (b) MoS<sub>2</sub>, (d) MoSe<sub>2</sub>, (e) WSe<sub>2</sub> layer and thickness of Ag (Au) thin film. The excitation wavelength for MoS<sub>2</sub>, MoSe<sub>2</sub> and WSe<sub>2</sub> is 1550, 1550, and 980 nm respectively coupled by SF11, BK7, and 2S2G prism.

performance. Among all these configurations, G-WS<sub>2</sub>(1)-G/Ag(42 nm) shows the highest sensitivity and an enhancement factor of over three orders.

The interactions between metal, graphene and TMDC materials could be assumed as the physical mechanism for the enhanced sensing performance: (i) the metal layer provides abundant free electrons for the excitation of surface plasmon polaritons; (ii) the efficiency of exciton relaxation is enhanced attributed to the strong spin-orbit interfacial and localized Coulomb interactions between TMDC materials and graphene layer, which leads to a higher light absorption rate<sup>[50,51]</sup>; (iii) more free electrons are transferred to the sensing surface to enhance the resonant electric field due to interlayer coupling, leading to the perfect absorption of the incident light and related phase jump<sup>[52]</sup>; (iv) more energy is transferred to afford the resonant oscillations of the free electrons on the sensing surface due to the efficient light absorption of graphene and TMDC materials; (v)

more electrons can be transferred to the sensing surface to participate in the resonant oscillations. This is attributed to the work function difference between metal, graphene and TMDC (i.e., Au-5.54 eV, MoS<sub>2</sub>-5.1 eV, graphene-4.5 eV), since the continuity of the Fermi levels of the whole system needs to be maintained.

## 4. Conclusion

In this study, G-TMDC-G hybrid metasurfaces for ultra-sensitive plasmonic biosensing have been systematically studied. The optimized G-TMDC-G/metal sensing substrates for four types of TMDC materials (i.e., WS<sub>2</sub>, MoS<sub>2</sub>, MoSe<sub>2</sub>, and WSe<sub>2</sub>) were respectively engineered. Our analysis demonstrated that G-TMDC-G hybrid nanostructure could enhance the SPR sensing performance significantly under optimum conditions. A high

enhancement factor of more than 3 orders of magnitude for differential phase change of SPR biosensor was successfully achieved for G-WS<sub>2</sub>(1)-G/Ag(42 nm) hybrid sensing substrate, coupling by ZnSe prism at the 632.8 nm excitation wavelength. For the G-WS<sub>2</sub>-G hybrid metasurface, monolayer WS<sub>2</sub> is found to have the highest efficiency for the electron charge transferred to metallic sensing surface to enhance the electric field. The outer graphene layer can not only prevent the oxidation of the Ag thin film but also act as a capture unit for sensing specific biomolecules. More importantly, the mature synthesis and transfer technologies ensure the experimental feasibility of the plasmonic sensor based on G-TMDC-G hybrid nanostructure. Thus, this G-TMDC-G hybrid plasmonic metasurface shows a great potential in the detection of the analyte with small molecular weight or ultra-low concentration.

## Supporting Information

Supporting Information is available from the Wiley Online Library or from the author.

## Acknowledgements

This work was supported by the Singapore Ministry of Education (Grant Nos. Tier 2 MOE2010-T2-2-010 (M4020020.040 ARC2/11) and Tier 1 M4010360.040 RG29/10), NTU-NHG Innovation Collaboration Grant (No. M4061202.040), A\*STAR Science and Engineering Research Council (No. M4070176.040), and School of Electrical and Electronic Engineering at NTU.

## Conflict of Interest

The authors declare no conflict of interest.

## Keywords

biosensing, graphene-TMDC-graphene, metasurface, plasmonic

Received: August 4, 2017  
Published online: October 17, 2017

- [1] S. Zeng, D. Baillargeat, H. P. Ho, K. T. Yong, *Chem. Soc. Rev.* **2014**, 43, 3426.
- [2] S. Zeng, K. V. Sreekanth, J. Shang, T. Yu, C. K. Chen, F. Yin, D. Baillargeat, P. Coquet, H. P. Ho, A. V. Kabashin, K. T. Yong, *Adv. Mater.* **2015**, 27, 6163.
- [3] J. Homola, *Chem. Rev.* **2008**, 108, 462.
- [4] V. G. Kravets, F. Schedin, R. Jalil, L. Britnell, R. V. Gorbachev, D. Ansell, B. Thackray, K. S. Novoselov, A. K. Geim, A. V. Kabashin, A. N. Grigorenko, *Nat. Mater.* **2013**, 12, 304.
- [5] V. G. Kravets, F. Schedin, A. V. Kabashin, A. N. Grigorenko, *Opt. Lett.* **2010**, 35, 956.
- [6] S. Zeng, S. Hu, J. Xia, T. Anderson, X. Q. Dinh, X. M. Meng, P. Coquet, K. T. Yong, *Sens. Actuators B* **2015**, 207, 801.
- [7] F. Xia, H. Wang, D. Xiao, M. Dubey, A. Ramasubramaniam, *Nat. Photonics* **2014**, 8, 899.
- [8] M. Xu, T. Liang, M. Shi, H. Chen, *Chem. Rev.* **2013**, 113, 3766.
- [9] S. Z. Butler, S. M. Hollen, L. Cao, Y. Cui, J. A. Gupta, H. R. Gutierrez, T. F. Heinz, S. S. Hong, J. Huang, A. F. Ismach, E. Johnston-Halperin, M. Kuno, V. V. Plashnitsa, R. D. Robinson, R. S. Ruoff, S. Salahuddin, J. Shan, L. Shi, M. G. Spencer, M. Terrones, W. Windl, J. E. Goldberger, *ACS Nano* **2013**, 7, 2898.
- [10] F. Schwierz, J. Pezoldt, R. Granzner, *Nanoscale* **2015**, 7, 8261.
- [11] I. Abid, A. Bohloul, S. Najmaei, C. Avendano, H. L. Liu, R. Pechou, A. Mlayah, J. Lou, *Nanoscale* **2016**, 8, 8151.
- [12] X. Duan, C. Wang, A. Pan, R. Yu, X. Duan, *Chem. Soc. Rev.* **2015**, 44, 8859.
- [13] D. Jariwala, V. K. Sangwan, L. J. Lauhon, T. J. Marks, M. C. Hersam, *ACS Nano* **2014**, 8, 1102.
- [14] Q. H. Wang, K. K. Zadeh, A. Kis, J. N. Coleman, M. S. Strano, *Nat. Nanotechnol.* **2012**, 7, 699.
- [15] A. K. Geim, *Science* **2009**, 324, 1530.
- [16] S. H. Choi, Y. L. Kim, K. M. Byun, *Opt. Express* **2011**, 19, 458.
- [17] V. G. Kravets, R. Jalil, Y. J. Kim, D. Ansell, D. E. Aznakayeva, B. Thackray, L. Britnell, B. D. Belle, F. Withers, I. P. Radko, Z. Han, S. I. Bozhevolnyi, K. S. Novoselov, A. K. Geim, A. N. Grigorenko, *Sci. Rep.* **2014**, 4, 5517.
- [18] Y. Chen, C. Tan, H. Zhang, L. Wang, *Chem. Soc. Rev.* **2015**, 44, 2681.
- [19] C. N. R. Rao, H. S. S. R. Matte, U. Maitra, *Angew. Chem. Int. Ed* **2013**, 52, 13162.
- [20] Q. Ouyang, S. Zeng, L. Jiang, L. Hong, G. Xu, X.-Q. Dinh, J. Qian, S. He, J. Qu, P. Coquet, K.-T. Yong, *Sci. Rep.* **2016**, 6, 28190.
- [21] S. Balendhran, S. Walia, H. Nili, J. Z. Ou, S. Zhurkov, R. B. Kaner, S. Sriram, M. Bhaskaran, K. Kalantar-zadeh, *Adv. Funct. Mater.* **2013**, 23, 3952.
- [22] L. Britnell, R. M. Ribeiro, A. Eckmann, R. Jalil, B. D. Belle, A. Mishchenko, Y. J. Kim, R. V. Gorbachev, T. Georgiou, S. V. Morozov, A. N. Grigorenko, A. K. Geim, C. Casiraghi, A. H. Castro Neto, K. S. Novoselov, *Science* **2013**, 340, 1311.
- [23] O. L. Sanchez, D. Lembke, M. Kayci, A. Radenovic, A. Kis, *Nat. Nanotechnol.* **2013**, 8, 497.
- [24] K. F. Mak, C. Lee, J. Hone, J. Shan, T. F. Heinz, *Phys. Rev. Lett.* **2010**, 105, 136805.
- [25] A. K. Geim, K. S. Novoselov, *Nat. Mater.* **2007**, 6, 183.
- [26] R. R. Nair, P. Blake, A. N. Grigorenko, K. S. Novoselov, T. J. Booth, T. Stauber, N. M. R. Peres, A. K. Geim, *Science* **2008**, 320, 1308.
- [27] A. K. Geim, I. V. Grigorieva, *Nature* **2013**, 499, 419.
- [28] T. Georgiou, R. Jalil, B. D. Belle, L. Britnell, R. V. Gorbachev, S. V. Morozov, Y. J. Kim, A. Gholinia, S. J. Haigh, O. Makarovskiy, L. Eaves, L. A. Ponomarenko, A. K. Geim, K. S. Novoselov, A. Mishchenko, *Nat. Nanotechnol.* **2013**, 8, 100.
- [29] S. Szunerits, N. Maalouli, E. Wijaya, J. P. Vilcot, R. Boukherroub, *Anal. Bioanal. Chem.* **2013**, 405, 1435.
- [30] L. Wu, H. S. Chu, W. S. Koh, E. P. Li, *Opt. Express* **2010**, 18, 14395.
- [31] P. Subramanian, A. Lesniewski, I. Kaminska, A. Vlandas, A. Vasilescu, J. Niedziolka-Jonsson, E. Pichonat, H. Happy, R. Boukherroub, *Biosens. Bioelectron.* **2013**, 50, 239.
- [32] I. Pockrand, *Surface Sci.* **1978**, 72, 577.
- [33] B. Radisavljevic, A. Radenovic, J. Brivio, V. Giacometti, A. Kis, *Nat. Nanotechnol.* **2011**, 6, 147.
- [34] A. M. Zande, P. Y. Huang, D. A. Chenet, T. C. Berkelbach, Y. You, G. H. Lee, T. F. Heinz, D. R. Reichman, D. A. Muller, J. C. Hone, *Nat. Mater.* **2013**, 12, 554.
- [35] S. Najma, Z. Liu, W. Zhou, X. Zhou, G. Shi, S. Lei, B. I. Yakobson, J. C. Idrobo, P. M. Ajayan, J. Lou, *Nat. Mater.* **2013**, 12, 754.
- [36] Y. Zhang, Y. Zhang, Q. Ji, J. Ju, H. Yuan, J. Shi, T. Gao, D. Ma, M. Liu, Y. Chen, X. Song, H. Y. Hwang, Y. Cui, Z. Liu, *ACS Nano* **2013**, 7, 8963.
- [37] Y. Zhang, T. R. Chang, B. Zhou, Y. T. Cui, H. Yan, Z. Liu, F. Schmitt, J. Lee, R. Moore, Y. Chen, H. Lin, H. T. Jeng, S. K. Mo, Z. Hussain, A. Bansil, Z. X. Shen, *Nat. Nanotechnol.* **2014**, 9, 111.

- [38] J. S. Ross, P. Klement, A. M. Jones, N. J. Ghimire, J. Yan, D. G. Mandrus, T. Taniguchi, K. Watanabe, K. Kitamura, W. Yao, D. H. Cobden, X. Xu, *Nat. Nanotechnol.* **2014**, *9*, 268.
- [39] C. L. Wong, H. P. Ho, Y. K. Suen, S. K. Kong, Q. L. Chen, W. Yuan, S. Y. Wu, *Biosens. Bioelectron.* **2008**, *24*, 606.
- [40] H. P. Ho, W. C. Law, S. Y. Wu, C. Lin, S. K. Kong, *Biosens. Bioelectron.* **2005**, *20*, 2177.
- [41] S. Zeng, X. Yu, W. C. Law, Y. Zhang, R. Rui, X. Q. Dinh, H. P. Ho, K. T. Yong, *Sens. Actuators, B* **2013**, *176*, 1128.
- [42] W. C. Law, K. T. Yong, A. Baev, P. N. Prasad, *ACS Nano* **2011**, *5*, 4858.
- [43] X. Yin, L. Hesselink, *Appl. Phys. Lett.* **2006**, *89*, 261108.
- [44] L. L. Kegel, D. B. Boyne, K. S. Booksh, *Anal. Chem.* **2014**, *86*, 3355.
- [45] J. Canning, J. Qian, K. Cook, *Photonic Sens.* **2015**, *5*, 278.
- [46] N. Goswami, A. Kar, A. Saha, *Opt. Commun.* **2014**, *330*, 169.
- [47] P. K. Maharana, R. Jha, *Sens. Actuators, B* **2012**, *169*, 161.
- [48] R. Jha, A. K. Sharma, *J. Opt. A: Pure Appl. Opt.* **2009**, *11*, 045502.
- [49] S. Patskovsky, A. V. Kabashin, M. Meunier, J. H. T. Luong, *Appl. Opt.* **2003**, *42*, 6905.
- [50] Z. Wang, D. K. Ki, H. Chen, H. Berger, A. H. MacDonald, A. F. Morpurgo, *Nat. Commun.* **2015**, *6*, 8339.
- [51] E. C. T. O' Farrell, A. Avsar, J. Y. Tan, G. Eda, B. Ozyilmaz, *Nano Lett.* **2015**, *15*, 5682.
- [52] C. E. Giusca, I. Rungger, V. Panchal, C. Melios, L. Zhong, Y. C. Lin, E. Kahn, A. L. Elias, J. A. Robinson, M. Terrones, O. Kazakova, *ACS Nano* **2016**, *10*, 7840.